Journal of Magnetic Resonance **149,** 22–28 (2001)
doi:10.1006/jmre.2000.2279, available online at http://www.idealibrary.com on IDEAL®

Magnet Design with High B_0 Homogeneity for Fast-Field-Cycling NMR Applications

O. Lips, A. F. Privalov, S. V. Dvinskikh,* and F. Fujara

*Fachbereich Physik, TU Darmstadt, 64289 Darmstadt, Germany; and *Physical Institute of St. Petersburg University, 198904 St. Petersburg, Russia*
E-mail: oliver.lips@physik.tu-darmstadt.de

Received July 10, 2000; revised November 27, 2000

The design, construction, and performance of a low-inductance solenoidal coil with high B_0 homogeneity for fast-field-cycling NMR is presented. It consists of six concentric layers. The conductor width is varied to minimize the B_0 inhomogeneity in the volume of the sample. This is done using an algorithm which takes the real shape of the conductor directly into account. The calculated coil geometry can be manufactured easily using standard computerized numeric control equipment, which keeps the costs low. The coil is liquid cooled and produces a B_0 field of 0.95 T at 800 A . The field inhomogeneity in a cylindrical volume (diameter 5 mm, length 10 mm) is about 10 ppm, and the inductance is 190 μH. Switching times below 200 μs can be achieved. During 6 months of operation the coil has shown good stability and reliability.

1. INTRODUCTION

Field cycling (FC) NMR is an acknowledged method for the study of field-dependent spin effects. In contrast to conventional NMR, the external magnetic field is varied during an experiment although the signal detection is always performed in a high, constant field. Thus field-dependent effects can be studied keeping the sensitivity of conventional NMR and without changing the spectrometer setup.

FC permits a great variety of applications: obtaining detailed information on the spectral density of fluctuating spin interactions (*1–3*), zero field spectroscopy (*4–6*), nuclear quadrupole double resonance spectroscopy (*7*), NQR imaging (*8, 9*), field cycling EPR (*10, 11*). Recently, the use of FC NMR has been shown to provide access to diffusion measurements under magic-angle field rotation conditions (*12*).

Based on Redfield's pioneering concept (*13*), a variety of FC techniques have been developed. Significant progress has been achieved in the past decade based on the optimization of the magnet system and the use of modern semiconductors (*14–18*). Recently the first commercial apparatus has become available (*19*). Nevertheless, the requirements for FC magnets, i.e., a high magnetic field, reasonable field homogeneity, and short switching times, are highly interrelated and render the magnet coil design complicated. However, the magnet design is crucial for the performance of the FC spectrometer.

The combination of a high magnetic field and fast switching can be realized best by small cylindrical coils (*1*), but since the B_0 field of a short solenoid shows a significant decrease away from the coil center, the resulting homogeneity is not sufficient for many applications. To overcome this limitation, several coil modifications have been reported (*1, 5, 15, 17, 20*). The idea of these designs is to correct the inhomogeneity in the axial direction by varying the current density along the coil axis. This can be done by adding extra turns (*1, 20*), by using a variable pitch angle (*17*), by varying the coil diameter (*5*), or by using a ribbon with continuously variable width (*15, 16*). In principal the last design is the most favorable one, but so far it is only realized using an algorithm (*15*) which takes into account an axial distribution of ring currents instead of currents following the real helical form of the conductor. After the optimization, the ring currents are transformed into a proper helix under the assumption that the homogeneity is preserved. It is evident that this procedure is not optimal if a homogeneity is required of the order of a few parts per million.

The need of an effective algorithm to improve the homogeneity is also enforced by the fact that low-inductance coils are preferred for FC. This means that it must be possible to achieve a sufficient homogeneity although only a few n turns per coil layer are used (inductance $\propto n^2$).

Here we describe a new approach to design a magnet for fast-field-cycling applications with optimized homogeneity of the B_0 field and low inductance. It avoids the disadvantage mentioned above, since the conductor geometry is taken directly into account. It will be shown that, even for coils with 19 windings, good results can be achieved. Furthermore, the coil design is appropriate for machining on a standard computerized numeric control (CNC) tool, which reduces the costs.

2. DESIGN AND OPTIMIZATION

The basic coil parameters, i.e., the number of coil layers, the number of turns per layer, the lengths, the radii, the thicknesses, and the gaps between the turns, were determined as described in Appendix A. A coil with six layers was found to be the optimum. The exact parameters are listed in Table 1.

1090-7807/01 $35.00

TABLE 1
Basic Coil Parameters

Layer	Turns	Inner radius (mm)	Thickness (mm)	Gap width (mm)
1	20	19.50	1.80	0.6
2	20	21.80	2.00	0.7
3	19	24.30	2.20	0.8
4	19	27.00	2.40	0.8
5	19	29.90	2.80	1.0
6	19	33.20	3.00	1.0

Note. The length of all layers is 100 mm.

The optimization of homogeneity was performed using an improved version of the algorithm described in (*21*). The shape of the conductor is given by its upper and lower boundaries which are determined by the functions $h_1(\phi)$ and $h_2(\phi)$. This is illustrated in Fig. 1, where as an example the fifth coil layer and the width of its unwrapped ribbon as a function of ϕ are shown. The angle ϕ is defined by the number of turns n and varies from $-n\pi$ to $n\pi$. The functions $h_1(\phi)$ and $h_2(\phi)$ are themselves specified by a Chebychev polynomial expansion $z(\phi)$ up to sixth order (see Eqs. [4]–[7] in Appendix B and Fig. 1). All together, the accurate shape of the wire is exactly determined by the expansion coefficients a_i of $z(\phi)$ and the fixed parameters radius, length, thickness, number of turns, and the gap between the turns.

The magnetic field for a specified shape of the conductor, i.e., for a given set of expansion coefficients a_i, can be calculated using the law of Biot–Savart (see Appendix B).

To optimize the homogeneity the mean squared relative deviation of the magnetic field at certain target points $B_z(\mathbf{r}_i)$ from the field in the center of the coil $B_z(0, 0, 0)$ was calculated:

$$\sigma = \frac{1}{N}\sum_{i=1}^{N}\left(\frac{B_z(\mathbf{r}_i)}{B_z(0,0,0)} - 1\right)^2. \qquad [1]$$

The deviation was minimized by varying the coefficients a_i using a Nelder–Mead minimization algorithm provided by the computer program MATLAB. We used nine target points on the coil axis at $z = 2, 3, \ldots, 10$ mm, which is sufficient for a homogeneous region of ± 10 mm in axial direction. In order to achieve a rapid field decrease toward the ends of the coil, a further target point $\mathbf{r}_{N+1}$, away from the coil center, was included in Eq. [1] which was set to half of $B_z(0, 0, 0)$ and weighted with an empirical reduction factor. In this way the stray field of the coil and thus the inductance could be reduced.

All six coils were optimized individually, mainly for pragmatic reasons. The limited number of free parameters in an individual fit kept the computing time short (about 1 day per layer using a Pentium 200 MHz). Furthermore, it was of advantage for our prototype that all layers are independent of each other and could be tested separately. The calculated resistances and the magnetic field strengths are collected in Table 2.

The achieved homogeneity is illustrated in Fig. 2, where the field profile in the $x - z$ plane at $y = 0$ for the assembled coil is shown. It can be seen that the calculated inhomogeneity on the

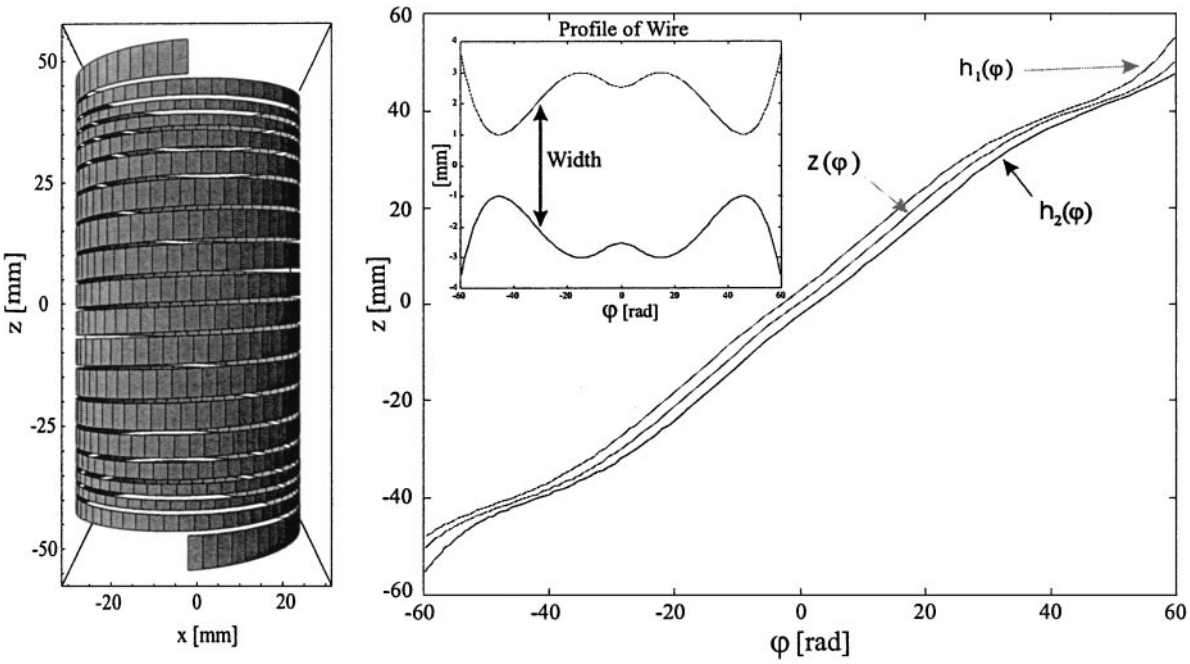

FIG. 1. Illustration of the mathematical description of the coil. As an example, the fifth coil layer (left) and its unwrapped ribbon (right) are shown. The ribbon is given by the boundary functions $h_1(\phi)$ and $h_2(\phi)$, which are themselves determined by the function $z(\phi)$. The inlay clarifies the resulting variation of the conductor width.

TABLE 2
Resistance, Inductance, and Magnetic Field Strength of the Coil

	Calculated		Measured		
Layer	Resistance (mΩ)	B(1000 A) (T)	Resistance (mΩ)	B(1000 A) (T)	Inductance (μH)
1	5.50	0.224	5.8	—	7.2
2	5.76	0.219	6.0	—	8.5
3	5.35	0.195	5.6	—	9.0
4	5.73	0.198	6.1	—	8.4
5	5.95	0.180	6.1	—	9.7
6	5.54	0.171	6.8	—	11.6
Total	34.83	1.188	36.6[a]	1.187[a,b]	188[a]

[a] Measured values of the assembled coil (not the algebraic sum of individual layers).
[b] Extrapolated from 800A.

coil axis ($x, y = 0$) is below 5 ppm. Even at the edges of the considered plane it does not exceed 20 ppm.

The main advantage of the presented optimization technique is that we consider the exact conductor geometry. Other methods, e.g., (*22, 23*), calculate a continuous current density on a cylindrical surface, which must be transformed into a discrete conductor geometry. The last procedure can only be done approximately and is a severe problem for low-inductance coils with very few turns.

3. CONSTRUCTION AND MACHINING

In this section we go into some construction details which may save a lot of trial and error in looking for the optimal procedure of building such a magnet.

The coil is built of six individually manufactured layers, which are mounted coaxially. Each layer is realized by machining a groove with constant width into a copper tube. To achieve a low resistance, electrolytic copper (E-Cu) is used.

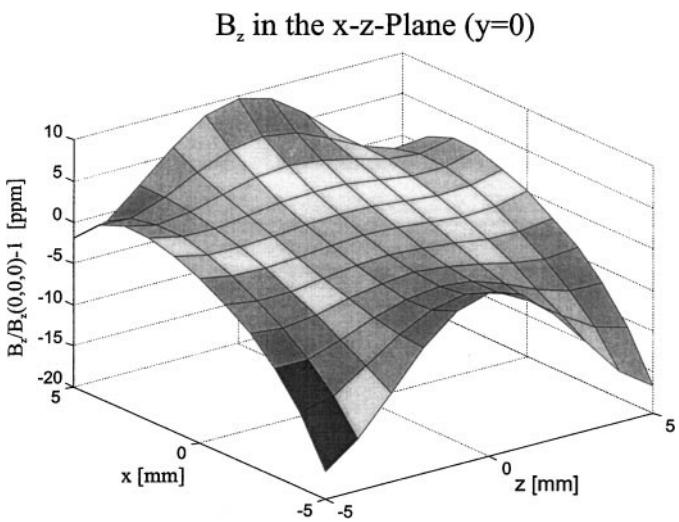

FIG. 2. Calculated field profile of the assembled coil in the $x - z$-plane at $y = 0$ ($z \parallel$ coil axis), given by the relative deviation from the field at the coil center in parts per million.

The main problem of machining the coil is to preserve the calculated homogeneity. Calculations show that especially an error in the diameter and the length of the coil cause a severe loss in homogeneity.

Since commercial copper tubes do not offer a sufficient accuracy, they were manufactured from thick copper cylinders using a lathe. To prevent machining errors caused by the torque of the chisel, the cylinder was glued (Pattex Stabilit) on an aluminium rod after machining the inner bore. The rod was chosen to be longer than the copper tube, so that the end of the rod could be lathed coaxially to the Cu cylinder. By fastening the end of the Al rod into the lathe, the outer diameter could be machined coaxially to the inner bore without any instabilities. In this way an accuracy of better than 0.01 mm for the diameters could be achieved easily. Furthermore, the rod was used as a substrate for further processing.

The groove between the windings was cut by a CNC milling machine (Hermle UWS 1000, Henninger Schnellfrässpindel) with an accuracy of 0.005 mm. The information for the milling machine was provided in pairs of the form (winding angle ϕ, z-position) which can be easily derived from Eq. [4]. Since the resistance of the coil depends on the cutting width, the mill should be as small as possible. So, the narrowest mills that could be found (HSC ALUMAX 2, Ritz GmbH Ennepetal) for a given conductor thickness were applied (see Table 1). More sophisticated cutting techniques like water jet cutting or spark erosion offer even smaller cuts, but at the expense of inconvenient handling and high costs. Since the influence of the gap width decreases with the number of windings (see Eq. [2]), we can avoid the use of these techniques for our design ($n \leq 20$). To compensate axial inhomogeneity caused by the helical structure, clockwise–anticlockwise cutting was used for consecutive layers. After milling the groove was fixed by T-shaped pertinax spacers (four to six spacers per turn), glued with epoxy resin (UHU endfest 300). The central aluminium core was excised and the remains of the Pattex stabilit glue were removed using acetone.

The rings which remain at the ends of each layer after milling were used to equal the overall coil lengths[1] to 120 mm. They are cut in the axial direction to avoid eddy currents during switching. The first and the last layer are furthermore soldered to copper rods which act as connections to the current source. The resistances and inductances of the machined coils are listed in Table 2.

Finally, all six coils were mounted coaxially and were serially connected by soldering (Fig. 3 left). The coils are installed in a

[1] The length L, which is used during the optimization process (100 mm), is defined by the value of $z(\phi)$ at the angles $n\pi$ and $-n\pi$ (see Fig. 1). The real length of the coil is given by the difference between the upper boundary $h_1(n\pi)$ and the lower boundary $h_2(-n\pi)$. Since the conductor width at the ends is different for each layer, the real coil length may vary slightly.

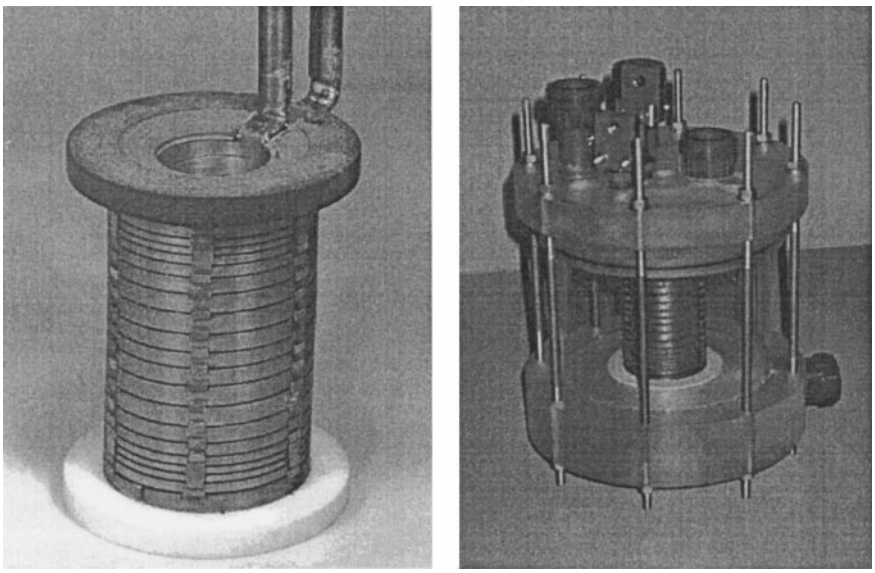

FIG. 3. Manufactured coil after soldering the individual layers (left) and after being assembled in its case (right).

Plexiglas case which provides sufficient stability. The assembled coil is shown in Fig. 3 (right).

4. COOLING

For our design we have chosen a cooling in the radial direction (see Fig. 4). A coolant flow of 15 $\frac{m^3}{h}$ perfluorpolyether (Galden HT 85) at a pressure of 2.5 bar is used. The coolant liquid enters the coil at the inside of the inner layer from the top and from the bottom and pours through the windings to the outside. We consider that this has some advantages compared to a flow in the axial direction used by other authors (*15, 16*):

- The flow is more turbulent, which enhances the heat transfer.
- There is no systematic heat gradient inside the coil in axial direction.
- The flow is strongest where most of the heat is produced, i.e., where the windings are densest.

The temperature of the coolant is kept around 12°C by a 50-kW plate heat exchanger (SWEP B12×70) which is cooled by water from an internal cooling circuit. Under a load of 800 A, the temperature in the conductor is stabilized after 2.5 s and is on average about 14° above that of the coolant.

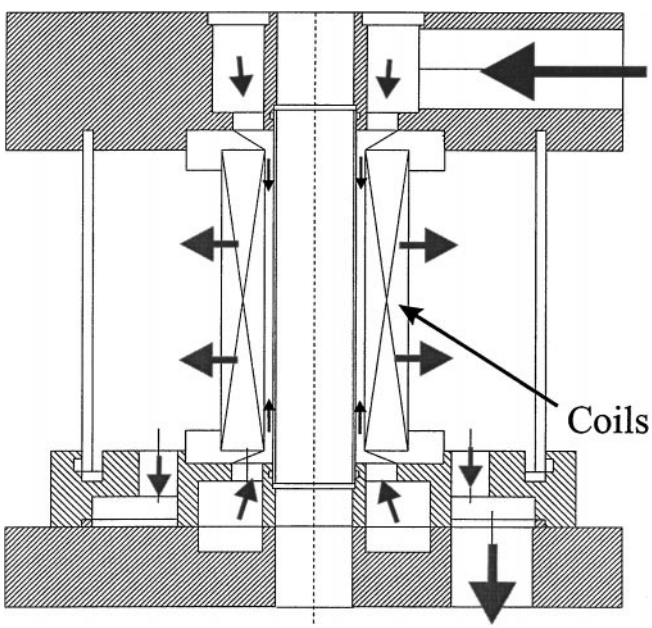

FIG. 4. Cooling flow schematically: Coolant enters the coil from the inside and pours through the windings to the outside.

5. PERFORMANCE OF THE COIL

The homogeneity of the constructed coil was tested experimentally by recording the NMR line width of a cylindrical water sample oriented perpendicular to the coil axis. The size was 5 mm in diameter and 10 mm in length. The signal was recorded at 39 MHz at room temperature. Since the T_2 of water is in the order of seconds, the decay of the ^{1}H signal (FID) is mainly determined by the field inhomogeneity. In Fig. 5 the observed FID is shown. The spectrum of the FID is presented in Fig. 6. The frequency scale is normalized with respect to the Larmor frequency ω_0. For comparison, the calculated field distribution in the proper volume is also displayed in Fig. 6. The measured inhomogeneity of approximately 10 ppm (defined by the linewidth at half height) is about three times above the calculated value

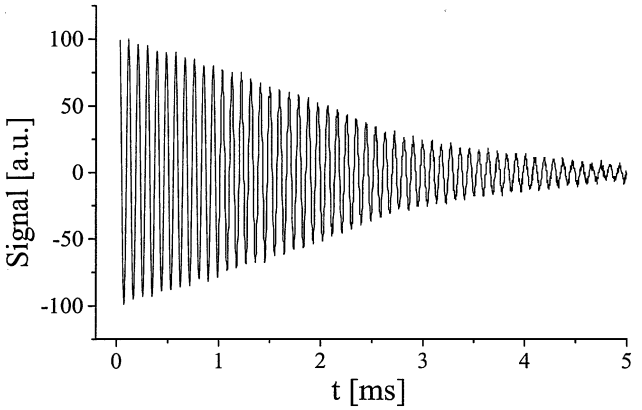

FIG. 5. Free induction decay of a water sample (diameter 5 mm, length 10 mm) at 39 MHz.

(≈3 ppm). The probable reasons are as follows:

- current density distributions inside the conductor caused by Lorentz forces and temperature gradients. These effects are not included in the optimization procedure;
- slight mechanical deformations of the coil caused by magnetic stresses and by thermal expansion;
- the limited precision of machining. Especially the accuracy of the first two coils suffered from the inexperience in manufacturing;
- the influence of the field from incoming and outgoing conductors.

Nevertheless, the experimental result is in good agreement with the calculation. A further improvement in homogeneity can be achieved by orientating the sample in the z-direction using a saddle-shape HF-coil and by applying shim coils.

The magnetic field that can be obtained with our present current source (modified AEG D30/600, 35 V, 800 A maximum, with homebuilt current regulation) is 0.95 T.

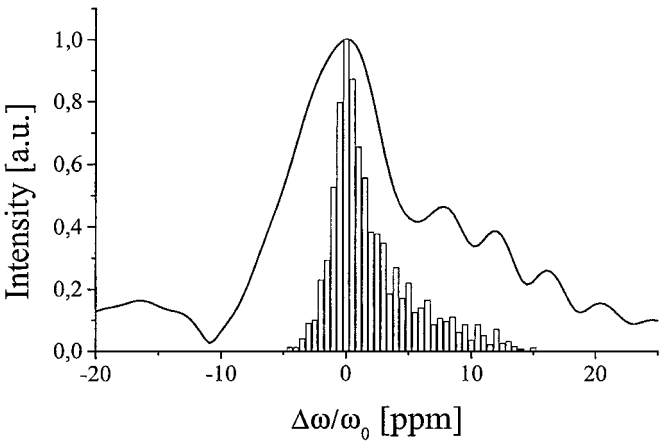

FIG. 6. Comparison of the measured lineshape (line) with the calculated field distribution (bars). For the calculation, 1700 equidistant points in the corresponding cylinder (5 mm diameter, 10 mm length) are considered.

The operation of our FC system during the first 6 months has shown that all parameters are stable.

6. SWITCHING

The switching is not the main topic of the current presentation. We use an energy storage switching circuit similar to that described in Ref. (*24*) realized with modern semiconducting devices. IGBTs of type Semikron SKM 400 GA 173 D are applied for switching and Power MOSFETs of type Advanced Power Technology APT 10M19BVR for current regulation. In this way switching times (i.e., the time to reach the new field value within 5% deviation) shorter than 0.2 ms can be achieved.

Even without the energy storage principle, i.e., using only the current regulation, the field transients are not longer than 6 ms.

7. CONCLUSION

We have described the design, construction, and performance of a magnet for field cycling applications. It features an easy to use optimization algorithm and it can be realized cost-effectively on standard CNC equipment. In contrast to other algorithms (*15, 20, 22, 23*), the exact wire geometry is taken directly into account during the optimization of homogeneity. The achieved homogeneity is about 10 ppm in a typical sample volume (cylinder of 5 mm diameter and 10 mm length) despite the relatively low number of turns. Due to the low inductance of the coil (190 μH), fast field transients can be achieved.

APPENDIX A

The basic parameters of our coil (number of layers, radii, number of turns, etc.) were chosen by estimating the magnetic field and the resistance of the coil.

The resistance R was approximated by dividing each layer into n rings with a cross section given by the length L of the coil minus the gaps between the windings:

$$R \approx \frac{2\pi r n^2 \rho}{d(L - nb)}. \qquad [2]$$

ρ denotes the specific resistance of electrolytic copper ($1.75\,10^{-8}$ Ωm), b the gap width, r the mean radius of the layer, d the thickness of the conductor, and n the number of turns. In this way the available current I for a given power source with voltage U (35 V in our case) could be calculated and thus the magnetic field. The field was approximated by using the standard formula for a thin solenoid with constant current density; any current distributions inside the conductor could be neglected for this purpose:

$$B_z(0,0,0) \approx \frac{\mu_0 n}{L} \frac{I}{\sqrt{1 + \left(\frac{2r}{L}\right)^2}} = \frac{\mu_0 U}{2\pi\rho} \frac{d(L - nb)}{nLr\sqrt{1 + \left(\frac{2r}{L}\right)^2}}. \qquad [3]$$

On this basis the configuration with the highest magnetic field could be found, taking into account the following constraints:

- a current not exceeding 1000 A,
- the minimal space needed for the probehead,
- the available cutting devices,
- a comparable heat production in all layers,
- an even number of layers for homogeneity reasons.

For the final determination of the basic coil parameters, the technical effort also had to be considered. One must judge whether a slightly greater magnetic flux may be justified by a more complicated construction and optimization. In our case we decided that it is not worth it to increase the number of layers to more than six.

APPENDIX B

The conducting wire is described on a cylindrical surface by two boundary functions, $h_1(\phi)$ and $h_2(\phi)$, depending on the angle ϕ. These functions are represented in the form

$$h_1(\phi) = \frac{z(\phi + 2\pi) + z(\phi)}{2} - \frac{b}{2} \qquad [4]$$

$$h_2(\phi) = \frac{z(\phi - 2\pi) + z(\phi)}{2} + \frac{b}{2}. \qquad [5]$$

The function $z(\phi)$ is given as a superposition of modified (see below) Chebychev polynominals up to the sixth order, which was found to be sufficient for the desired homogeneity:

$$z(\phi) = k \sum_{i=1}^{6} a_i T_i(\phi), \qquad [6]$$

with $a_1 = 1$ and $z(n\pi) = \frac{L}{2}$. The normalizing parameter k keeps the coil length fixed. The Chebychev polynominals are given by the known formula (*25*),

$$T_0(\phi) = 1; \quad T_1(\phi) = \phi; \quad T_{n+1}(\phi) = 2\phi T_n(\phi) - T_{n-1}(\phi), \quad [7]$$

but for symmetry reasons all terms containing even powers of ϕ were multiplied by sign(ϕ).

During the optimization procedure the parameters a_i ($i = 2 \ldots 6$) were varied.

The magnetic field in axial direction B_z was calculated using the law of Biot–Savart for a superposition of currents flowing between the boundary functions $h_1(\phi)$ and $h_2(\phi)$:

$$B_z(x_i, y_i, z_i) = \frac{\mu_0 I}{4\pi \ln \frac{r_a}{r_i}} \int_{r_i}^{r_a} \int_{-n\pi}^{n\pi} \int_{h_2(\phi)}^{h_1(\phi)} \frac{1}{h_1(\phi) - h_2(\phi)} \times \frac{r - (y_i \sin(\phi) + x_i \cos(\phi))}{[(x_i - r\cos(\phi))^2 + (y_i - r\sin(\phi))^2 + (z_i - z)^2]^{\frac{3}{2}}} \, dz \, d\phi \, dr. \qquad [8]$$

Thereby an additional $\frac{1}{r}$ current distribution in radial direction between the inner (r_i) and outer (r_a) radii, caused by the coil resistance, is also considered (*26*). Field components in the radial direction are not taken into account since they are small and at least partially cancelled by the opposite helicity of two consecutive layers.

ACKNOWLEDGMENTS

We thank the mechanical workshop of the Fachbereich Physik (Universität Dortmund, Germany), especially G. Ernst, H. Noffke, J. Mellentin, and D. Buß, for machining all components of the coil.

REFERENCES

1. F. Noack, NMR-field cycling spectroscopy: Principles and applications, *Progr. Nucl. Magn. Reson. Spectrosc.* **18,** 171–276 (1986).
2. R. Kimmich, "NMR Tomography, Diffusometry, Relaxometry," Springer-Verlag, Berlin (1997).
3. A. F. Privalov, S. V. Dvinskikh, F. Fujara, and H.-M. Vieth, Frequency-dependent spin–lattice relaxation study of transport processes in superionic conductors, *Appl. Magn. Reson.* **15,** 353–361 (1998).
4. A. Bielecki, D. B. Zax, K. W. Zilm, and A. Pines, Zero-field NMR and NQR spectrometer, *Rev. Sci. Instrum.* **57**(3), 393–403 (1986).
5. M. V. Terekhov and S. V. Dvinskikh, Magnetic system for zero-field ^{1}H NMR measurements, *Instrum. Exp. Techniques* **39**(3), 145–150 (1996).
6. D. B. Zax, A. Bielecki, K. W. Zilm, A. Pines, and D. P. Weitekamp, Zero field NMR and NQR, *J. Chem. Phys.* **83**(10), 4877–4905 (1985).
7. D. T. Edmonds, Nuclear quadrupolar double resonance, *Phys. Rep.* **29**(4), 233–290 (1977).
8. Y. Lee, D. C. Michaels, and L. G. Butler, ^{11}B imaging with field-cycling NMR as a line narrowing technique, *Chem. Phys. Lett.* **206**(5, 6), 464–466 (1993).
9. Y. Lee and L. G. Butler, Field-cycling ^{14}N NQR imaging with spatial and frequency resolution, *J. Magn. Reson. A* **112,** 92–95 (1995).
10. J. Krzystek, M. Notter, and A. L. Kwiram, Field-cycled electron double resonance, *J. Phys. Chem.* **98**(14), 3559–3561 (1994).
11. G. Sturm, A. Lötz, and J. Voitländer, Pulsed EPR with field cycling and a bridged loop–gap resonator made by chemical deposition of silver, *J. Magn. Reson.* **127,** 105–108 (1997).
12. F. Noack, S. Becker, and J. Struppe, Applications of field-cycling NMR, *Annu. Rep. NMR Spectros.* **33,** 1–36 (1997).
13. A. G. Redfield, W. Fite II, and H. E. Bleich, Precision high speed current regulators for occasionally switched inductive loads, *Rev. Sci. Instrum.* **39**(5), 710–715 (1968).
14. E. Rommel, K. Mischker, G. Osswald, K.-H. Schweikert, and F. Noack, A powerful NMR field-cycling device using GTOs and MOSFETs for relaxation dispersion and zero-field studies, *J. Magn. Reson.* **70,** 219–234 (1986).
15. K.-H. Schweikert, R. Krieg, and F. Noack, A high-field air-cored magnet coil design for fast-field-cycling NMR, *J. Magn. Reson.* **78,** 77–96 (1988).
16. M. Blanz, T. J. Rayner, and J. A. S. Smith, A fast field-cycling NMR/NQR spectrometer, *Meas. Sci. Technol.* **4,** 48–59 (1993).
17. C. Job, J. Zajicek, and M. F. Brown, Fast field cycling nuclear magnetic resonance spectrometer, *Rev. Sci. Instrum.* **67**(6), 2113–2122 (1996).

18. D. M. Sousa, E. Rommel, J. Santana, J. Silva, J. Fernando, P. J. Sebastião, and A. C. Ribeiro, Power supply for fast field cycling NMR spectrometer using IGBTs operating in the active zone. *In* "Proceedings of the 7th European Congress on Power Electronics and Applications," Vol. 2, pp. 2.285–2.290, Trondheim, September 1997.

19. STELAR s.n.c., Mede (Italien). "Spinmaster-FFC Fast Field Cycling NMR Relaxometer," Prospectus (1998).

20. G. Grössl, F. Winter, and R. Kimmich, Optimisation of magnet coils for NMR field-cycling experiments, *J. Phys. E: Sci. Instrum.* **18,** 358–360 (1985).

21. A. F. Privalov, S. V. Dvinskikh, and H.-M. Vieth, Coil design for large-volume high-B_1 homogeneity for solid state NMR applications, *J. Magn. Reson.* **123,** 157–160 (1996).

22. R. Turner, A target field approach to optimal coil design, *J. Phys. D: Appl. Phys.* **19,** L147–L151 (1986).

23. R. Turner, Minimum inductance coils, *J. Phys. E: Sci. Instrum.* **21,** 948–952 (1988).

24. M. Blanz, "'Field-Cycling"'-Kernspinresonanzanlage und ultraschnelles Abschrecken im flüssigen Helium zur Untersuchung von Wasserstoff in Metallen. Ph.D. thesis, Max-Planck-Institut für Metallforschung, Stuttgart, (1989).

25. I. N. Bronstein, K. A. Semendjajew, G. Musiol, and H. Mühlig, "Taschenbuch der Mathematik," Verlag Harri Deutsch (1993).

26. D. B. Montgomery, "Solenoid Magnet Design: The Magnetic Aspects of Resistive and Superconducting Systems," Wiley, New York (1969).